High-sensitivity specific heat study of the low-temperature–high-field corner of the H – T phase diagram of FeSe

T. Klein, A. Demuer, G. Seyfarth, H. Cercellier, L. Doussoulin, Pierre Toulemonde, A.-A. Haghighirad, F. Hardy, C. Marcenat

High-sensitivity specific heat study of the low-temperature–high-field corner of the H-T phase diagram of FeSe

T. Klein,[1,*] A. Demuer,[2] G. Seyfarth,[2] H. Cercellier,[1] L. Doussoulin,[1] P. Toulemonde,[1] A.-A. Haghighirad,[3] F. Hardy,[3] and C. Marcenat[4]

[1]*Université Grenoble Alpes, CNRS, Grenoble INP, Institut Néel, F-38000 Grenoble, France*

[2]*Université Grenoble Alpes, INSA Toulouse, Université Toulouse Paul Sabatier, CNRS, LNCMI, F-38000 Grenoble, France*

[3]*Institute for Quantum Materials and Technologies, Karlsruhe Institute of Technology, 76021 Karlsruhe, Germany*

[4]*Université Grenoble Alpes, CEA, INAC, PhELIQS, LATEQS, F-38000 Grenoble, France*

(Received 4 March 2023; revised 26 May 2023; accepted 30 May 2023; published 13 June 2023)

We report on an extensive experimental study of the low-temperature–high-field corner of the H-T phase diagram in FeSe using high-sensitivity specific heat C measurements. Indeed, the superconducting gap and Fermi and Zeeman energies are surprisingly close in this compound, possibly leading to the existence of different superconducting phases as well as Lifshitz transitions in the electronic structure. The nature of this part of the phase diagram hence remains debated, and we show here that two distinct anomalies are visible in $C(H)$ (below ∼3 K): a (smeared) jump at the superconducting transition and a kink in $C(H)$. This second structure lies either below (for H close to the ab plane) or above (for field orientations close to the c direction) the superconducting transition, indicating that it is most probably related to a field-induced change in the electronic structure. Moreover, quantum oscillations are clearly observed below ∼2 K, and $C(H)$ can be well described by the Lifshitz-Kosevich formula for fields both above and below the kink (with an effective mass $m^* \sim 4m_e$ and a frequency $F \sim 200$ T, in good agreement with the values previously inferred from magnetotransport measurements for the hole sheet).

DOI: 10.1103/PhysRevB.107.224506

I. INTRODUCTION

FeSe is a particularly interesting iron-based superconductor, composed only of c-axis stacking of FeSe layers without any charge reservoir. In contrast to other iron-based materials, this system does not order magnetically (but still undergoes a structural phase transition [1–3]), and superconductivity here competes with an orbitally ordered nematic state [4–6]. Moreover, despite its moderate critical temperature ($T_c \sim 9$K), FeSe can be seen as an *extremely* high T_c material due to its very low Fermi energy ϵ_F and corresponding carrier concentration. This Fermi energy is then comparable to the superconducting gap Δ_{SC}, and FeSe therefore lies at the verge of a BEC-BCS crossover ($k_F\xi \sim 1$, where k_F is the Fermi wave vector and ξ is the coherence length).

On the other hand, for magnetic fields close to the zero-T upper critical field $H_{c2}(0)$ (∼14 and ∼27 T for $H||c$ and $H||ab$, respectively [7]), Δ_{SC} is also comparable to the Zeeman energy [$\epsilon_Z = g\mu_B H_{c2}(0)$], hence favoring the formation of the Fulde-Ferrell-Larkin-Ovchinnikov (FFLO) state with Cooper pairs having finite momenta. Specific heat measurements confirmed that paramagnetic depairing reduces $H_{c2}(0)$ well below its orbital limit for $H||ab$, underlining the importance of paramagnetic effects [7], and the presence of a putative FFLO state was suggested by Kasahara *et al.* to account for anomalies in thermal conductivity measurements for both $H||ab$ [8] and $H||c$ [9]. The existence of this FFLO phase was also recently put forward [10] to account for the presence of a kink in the field dependence of the specific heat at low temperature for $H||c$.

However, the Zeeman energy is also of the order of the Fermi energy, questioning the validity of the FFLO scenario in this "exotic" superconducting state of highly spin-polarized electrons (see discussions in [8–11]). The existence of an inherent spin-density-wave instability related to field-induced nesting of the spin-polarized electron/hole Fermi sheets was alternatively proposed by Ok *et al.* [11] to account for anomalies observed in both the irreversible torque and magnetocaloric measurements for H close to the ab plane. Alternatively, as the Fermi sheets of the minority (electron and/or hole) spin species shrink with increasing field, it has been suggested [12] that one or both could disappear at high field while the other one would still exist, leading to magnetic-induced Lifshitz transitions.

The nature of the low-T–high-H corner of the phase diagram hence remains an open question. The presence of two characteristic fields was inferred from various experiments for both $H||c$ and $H||ab$, and following [8–10], a putative phase diagram is sketched as scenario A in Fig. 1, with an FFLO phase (phase B) separating the normal state (phase N) from the standard superconducting state (phase A) for all field directions. However, a detailed study of the angular dependence of the phase diagram deduced from thermodynamic (i.e., reversible) specific heat measurements is still lacking.

We performed an extensive study of this phase diagram down to ∼0.4 K and up to 36 T for various orientations of the magnetic field, using high-sensitivity AC specific heat

*thierry.klein@neel.cnrs.fr

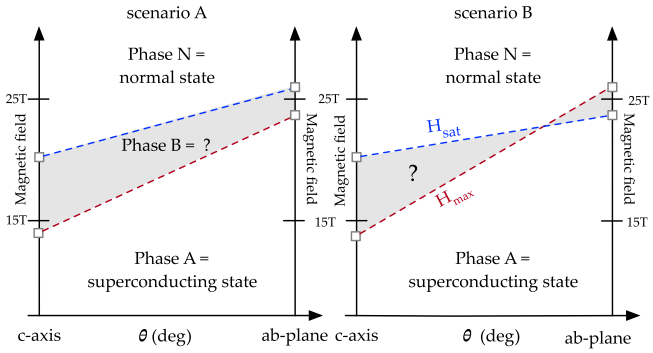

FIG. 1. Schematic low-temperature H-θ phase diagram of FeSe (θ is the angle between the magnetic field H and the c axis). Two anomalies (squares) were inferred in various measurements ([8–11] and present work) for both $H||ab$ and $H||c$. In scenario A (see [8–10]), a FFLO phase B separates the normal state (phase N) from the superconducting state (phase A) for all field directions. In scenario B, supported by the present work, the two lines cross, and the superconducting to normal state transition is delimited by the red line (labeled H_{max}; see Figs. 5–7 below). The origin of the second anomaly (labeled H_{sat}; see Figs. 5–7 below) still has to be clarified but might be related to changes in the electronic structure of the normal state.

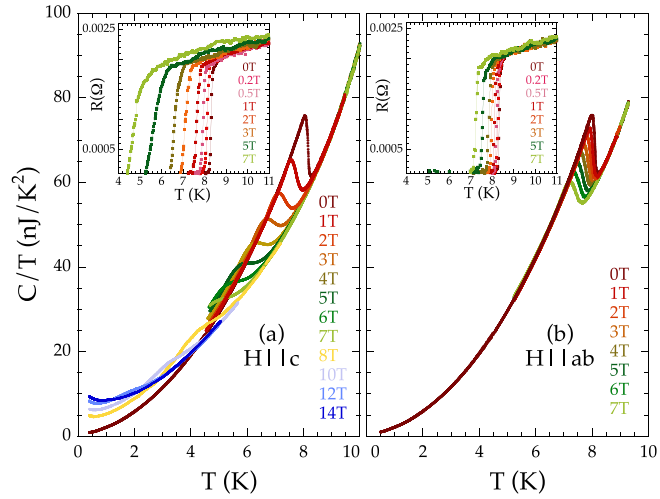

FIG. 2. Temperature dependence of the specific heat for (a) $H||c$ and (b) $H||ab$ (right panel) and for the indicated magnetic fields (sample 1). Corresponding resistive transitions are displayed in the insets. The small upturn in C/T at low T and large H is due to a small $C \propto (H/T)^2$ Schottky tail which has been subtracted from the data in the following figures.

measurements. Our data show that the kink previously reported by Kasahara *et al.* [8] in the field dependence of C/T is actually reminiscent of a clear (smeared) superconducting jump (for $H = H_{max}$; see Figs. 5–7 below), rather supporting scenario B in Fig. 1. Indeed, a second characteristic field (above which the normal state specific heat saturates, labeled H_{sat}; see Fig. 1 and also Figs. 5–7 below) is also clearly visible, but this field only very weakly depends on the angle θ between the magnetic field and the c axis. H_{sat} then lies above (for $\theta \to 0$) or below (for $\theta \to 90°$) the superconducting transition, reminiscent of the anomaly observed by Ok *et al.* [11] for this later field orientation. Our data indicate that this field is not related to superconductivity but might be attributed to a field-induced Lifshitz transition as proposed in [12].

II. SAMPLES AND EXPERIMENTS

FeSe single crystals were synthesized by chemical vapor transport [13–15] using a eutectic mixture of KCl and $AlCl_3$ and were characterized using x-ray diffraction (see also [16] for more details on the sample growth and characterization using different probes).

The total heat capacity was deduced using $C_p = P_{ac}\sin(-\phi)/2\omega|T_{ac}|$, where P_{ac} is a periodically modulated heating power, ϕ is the thermal phase shift, and T_{ac} is the induced temperature oscillations. A miniature Cernox resistive chip was split into two parts and attached to a small copper ring with PtW(7%) wires. The first half (R_H) was then used as an electrical heater [$P_{ac} = R_H i_{ac}(\omega)^2/2$], and the second half ($R_T$) was used to record the temperature oscillations [$V_{ac}(2\omega) = (dR_T/dT)T_{ac}(2\omega)i_T$, where i_T is the reading current]. In order to subtract the heat capacity of the sample mount (chip + a few micrograms of Apiezon grease used to glue the sample onto the back of the chip), the empty chip (with grease) was measured prior to the sample measurements. A precise *in situ* calibration and corrections of the thermometer magnetoresistance in magnetic field were included in the data treatment. This technique enabled us to obtain absolute values of the specific heat of miniature single crystals with an accuracy on the order of ∼95% (as deduced from measurements on ultrapure copper) and a signal-to-noise ratio up to $\sim 10^4$. Electrical resistivity in the ab plane of the crystals was measured by standard four-contact transport measurements under a magnetic field (up to 7 T) to estimate the temperature dependence of the vortex melting line (defined as $R = 0$) in both orientations (in the ab plane and along the c axis).

Two miniature (∼0.3 mg ≡ 0.05 mm^3) single crystals were measured with $T_c \sim 8.1$ and 9.0 K for samples 1 and 2, respectively. Both exhibit well-defined specific heat anomalies at the superconducting transition for $H = 0$, attesting to their high quality (see Fig. 2 for sample 1 and [7] for sample 2). As shown, the specific heat transition is progressively shifted by the magnetic field and significantly broadens as expected in the presence of large thermal fluctuations. In contrast, well-defined resistive transitions (see inset of Fig. 2) are observed up to 7 T, and the onset of resistivity (black symbols in Fig. 4 in below) lies close to the maximum of the specific heat, indicating that the resistivity in the vortex liquid state (see below) rapidly reaches its normal state value.

III. H-T PHASE DIAGRAM

A. Melting of the vortex solid ($T > 3$ K)

The H-T phase diagram of FeSe was previously investigated in detail in [7]. The existence of significant thermal fluctuations leading to the melting of the vortex matter was demonstrated, and the presence of an unusual behavior for fields parallel to the ab plane clearly indicated that the Pauli

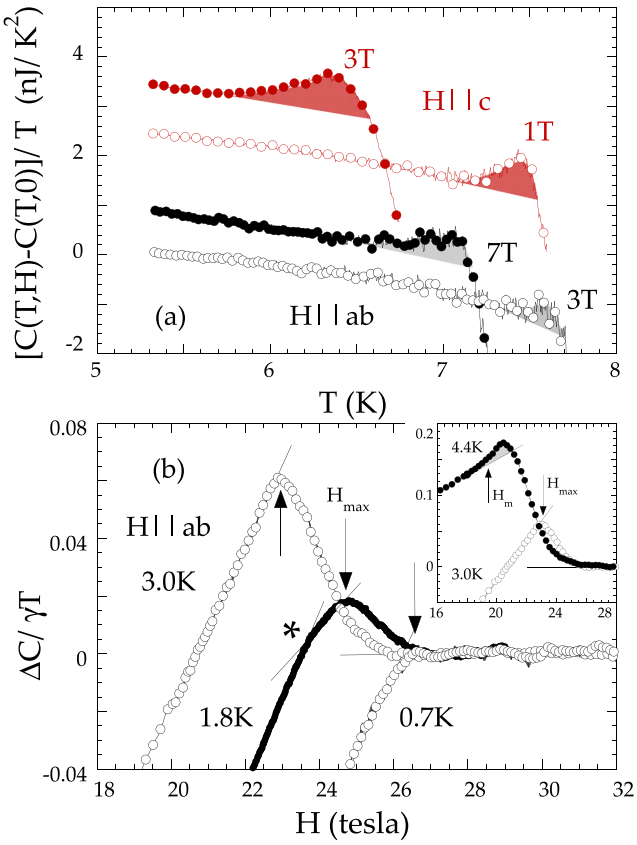

FIG. 3. (a) Specific heat of sample 1 as a function of temperature for $H||ab$ (black symbols) and $H||c$ (red symbols). To emphasize the bump at the melting anomaly (shaded area) the 0 T data have been subtracted from those obtained for the indicated H values (the data for $H||c$ are shifted by 2 nJ/mol K^2 for clarity). (b) Magnetic field dependence of the specific heat of sample 2 at low temperature for $H||ab$; no melting bump could be observed in this temperature range [see the inset for the data at 4.4 K for comparison; the melting bump is marked by the gray shaded area, and the melting field H_m (onset of the bump) is indicated by the vertical arrow], and C/T displays the standard smeared jump associated with the superconducting to normal state crossover. The $H_{\max}$ values (vertical arrows) are reported in Fig. 4 as solid symbols. Note the kink at $T = 1.8$ K marked by the star (see text for details).

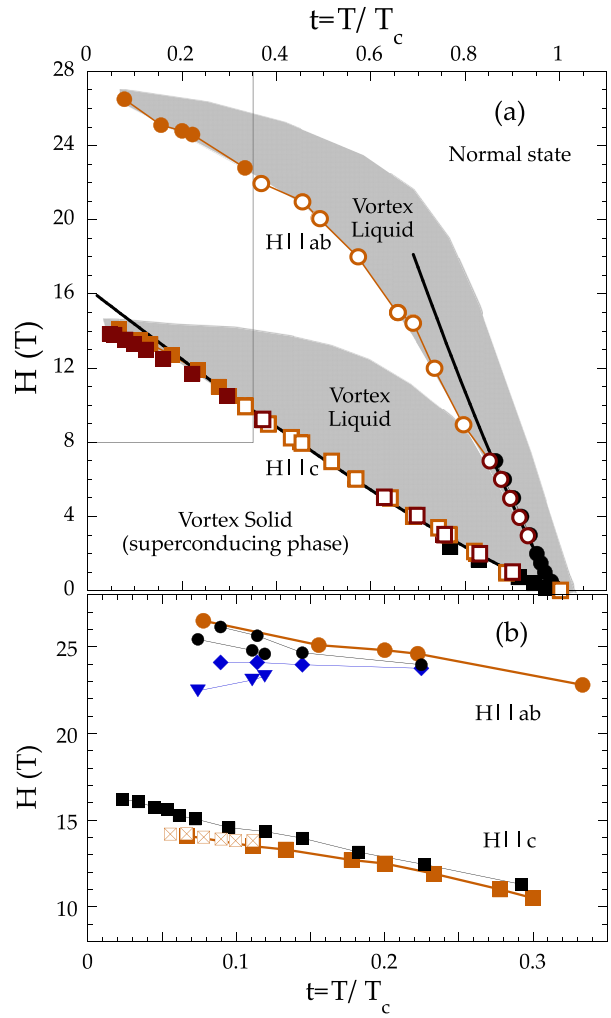

FIG. 4. (a) H-T phase diagram of FeSe. Open squares and circles (for $H||c$ and $H||ab$, respectively) correspond to the vortex melting line deduced from specific heat measurements in sample 1 (brown data) and sample 2 (orange data). The onset of the resistive transition is indicated by the black symbols, and the solid brown and orange symbols correspond to the maximum in the field dependence of C/T ($H_{\max}$ in Figs. 5–7). The gray shaded areas indicate the width of the superconducting "jump," here smeared by the thermal fluctuations (C/T reaches its normal state value only above those areas). The solid lines are fits to the data using a $(1-t)^{1.2}$ law with an anisotropy between the two directions, $\gamma \sim 4.5$ (see text for details). A zoom of the low-T–high-H corner of the phase diagram (dashed rectangular box) is displayed in (b). The orange symbols correspond to the maximum in the field dependence of C/T [as in (a)], and the black symbols correspond to the irreversibility line (from [10] for $H||c$ and [8,11] for and $H||ab$). The crossed squares correspond to the kink in $C/T(H)$ reported in [10], the blue triangles correspond to the locus of the magnetic torque anomaly (from [11]), and the lozenges correspond to the anomaly in thermal conductivity (from [8]).

limitation plays a significant role in this direction. Indeed, above ~3 K, a characteristic melting bump is visible in the temperature and field dependence of C/T (see Fig. 3(a) for sample 1 and Fig. 2 in [7] for sample 2). This broad discontinuity is reminiscent of the vortex-melting transition initially reported in twinned YBaCuO single crystals [17] (see also the discussion in [7]), and the locus of this anomaly is reported in Fig. 4 (open symbols) together with the onset of the resistive transition. As shown, very similar phase diagrams were obtained for the two samples despite their different T_c values, and the bump for $H\|ab$ which was initially not resolved below 7 T in sample 2 [7] could be observed down to ~3 T in sample 1 [see Fig. 3(a)].

The width of the fluctuation regime is indicated by the gray shaded areas in Fig. 4 (C/T reaches its normal state value only above this area). Note that the transition becomes *extremely* large at low temperature ($\Delta T/T \sim 2$–3), which may be an indication of strong *critical* fluctuations associated with the very low condensation energy [18] of FeSe, $\epsilon_{\rm cond} = (\Phi_0/4\pi\mu_0\lambda_{ab})^2\xi_c \sim 70$ K (λ_{ab} and ξ_c are the in-plane penetration depth and out-of-plane correlation length, respectively). The Ginzburg number, measuring the strength of the

thermal fluctuations [19,20], $G_i = (1/8)(k_B T_c/\epsilon_0 \xi_c)^2 \sim 10^{-3}$, is then on the order of the one observed in high-T_c superconductors (as a comparison $G_i \sim 10^{-8}$ in Nb with similar T_c and $\sim 5.10^{-3}$ in YBaCuO [19]), leading to the melting of the vortex solid [7], as previously observed in high-T_c materials [19–21].

The temperature dependence of the melting field can then be calculated assuming that the lattice displacement in the presence of thermal (and/or quantum) fluctuations becomes on the order of $\sim c_L$ times the vortex lattice spacing for $H = H_m(T)$ [19,20] (where c_L is the Lindemann constant, ~0.2–0.3; see discussion in [7]). For, $t = T/T_c \to 1$, this melting field is expected to vary as

$$H_m \propto [(1-t)/t]^2/[1+\sqrt{1+4S(1-t)/t^2}]^2,$$

with $S \sim S_{th} \sim 5c_L^4/G_i$ in the case of thermal fluctuations, and H_m can be well approximated by an $H_m \propto (1-t)^\alpha$ power law with $\alpha < 2$, decreasing for increasing S_{th} values [21–25]. As shown in Fig. 4 (solid lines), such a simple power law approximation also leads to good agreement with the data in FeSe with $\alpha \sim 1.2 \pm 0.1$ for both field directions. This α value corresponds to $S_{th} \sim 30$, in reasonable agreement with the approximate value (~20) that can be estimated taking $G_i = 10^{-3}$ and $c_L = 0.25$. Note that an extra contribution to S may arise from quantum fluctuations $S_Q \sim [c_L^2/G_i^{0.5}] \times [\beta_Q/k_F\xi]$, with $\beta_Q \approx 7$–35 [22]. Here S_Q is of the order of 4-20 due to the small $k_F\xi$ value, which could further contribute to the small α value (as $S = S_{th} + S_Q$), but the uncertainty on c_L unfortunately hinders any further discussion of the influence of this contribution.

This simple power law approximation surprisingly holds down to very low temperatures even though it is based on a Ginzburg-Landau approximation (see, for instance, [21]), and here it well describes the $H_m(T)$ line down to $T \sim 2$ K for $H||c$. Extrapolating this line for $T \to 0$ then suggests that the (orbital) critical field $H_{orb}^{||c}(0)$ is of the order of ~16.5 T for $H||c$ (see discussion below). No melting anomaly could be observed below ~3K (in either direction), probably due to the presence of residual static disorder [20], which could be related to nematic domain walls [26], but $H_m(T)$ can still be well fitted down to the lowest temperatures, going beyond this Ginzburg-Landau approximation and introducing corrections to the upper critical field due to paramagnetic effects [7] (assuming that, in the absence of disorder, the melting of the vortex solid would lie close to the field H_{max} corresponding to the maximum in C/T; solid symbols in Fig. 4).

Those paramagnetic corrections are then very strong for $H||ab$ (see discussion in [7]), leading to deviations from the power law line [27] already below ~7 T and, correspondingly, to an $H_{c2}^{||ab}(0)$ value on the order of 27 T, which is much smaller than the orbital value $H_{orb}^{||ab} \sim \gamma \times 16.5 \sim 75$ T, where $\gamma \sim 4.5$ is the anisotropy of the melting lines for $T \to T_c$ (i.e., of the power law lines).

B. Superconducting transition at low T ($T < 3$ K)

Even though no true thermodynamical phase transition could be observed at low temperature, the specific heat displays a clear (smeared) jump below 3 K [see Fig. 3(b) for $H||ab$], as expected for the superconducting transition in the presence of thermal fluctuations. As is usually observed, the amplitude of this jump decreases with T and here finally vanishes below 0.7 K for $H||ab$ but remains visible down to the lowest temperatures for $H||c$ (see Figs. 5 and 6). Most of the ordering energy comes out [28,29] at the C/T maximum, and H_{max} then lies in the vicinity of the underlying mean field H_{c2}^{MF} line. As a comparison, the melting anomaly observed at higher temperatures (4.4 K, for example) is displayed in the inset (gray shaded area). Note that a clear (small) change in slope is visible in $C/T(H)$ around ~24 T (i.e., below H_{max}) for $T = 1.8$ K [see star in Fig. 3(b)], which will be discussed later.

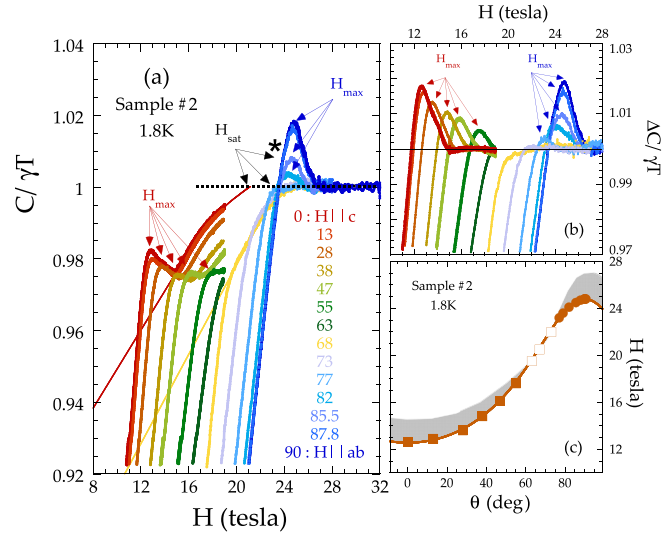

FIG. 5. (a) Magnetic field dependence of the specific heat in a FeSe single crystal (sample 2) at $T = 1.8$ K for the indicated values of the angle θ between the field and the c axis. Note that no increase of C/T *above* H_{max} is observed for $\theta \gtrsim 80°$, but a clear kink remains visible *below* H_{max} in this angle range [marked by the star; see also Fig. 3(b)]. (b) Same as (a) after subtraction of a smooth background [thin red to yellow lines in (a)], emphasizing the similarity of the superconducting anomaly for $\theta \to 0$ and $\theta \to 90°$. (c) Angular dependence of the maximum (solid squares) or kink in the intermediate angular range (open squares; the gray shaded areas indicate the width of the fluctuation regime). $H_{max}(\theta)$ can be well described by a standard $H_{max}(\theta) = H_{max}^{||ab}/\sqrt{[\tilde{\gamma}\cos(\theta)]^2 + [\sin(\theta)]^2}$ law for anisotropic superconductors with $\tilde{\gamma} \sim 2$ (solid line; see the discussion in text).

To further study the superconducting transition, the chip was mounted on a piezoelectric rotator in order to measure the field dependence of C/T for various angles θ between the c axis and the magnetic field (at $T = 1.8$ K). As shown in Fig. 5, the superconducting overshoot progressively disappears with decreasing angle (and shifts towards lower fields) and finally vanishes for $55° \lesssim \theta \lesssim 75°$, giving rise to a kink in C/T vs H. The absence of the superconducting jump in this angle range remains to be explained, but an overshoot again develops below to $\theta \sim 50°$. However, in this latter angle range a *minimum* surprisingly develops in $C/T(H)$ above H_{max}, and C/T increases above the superconducting transition, finally saturating only for $H \gtrsim H_{sat} \gg H_{max}$ (see discussion below).

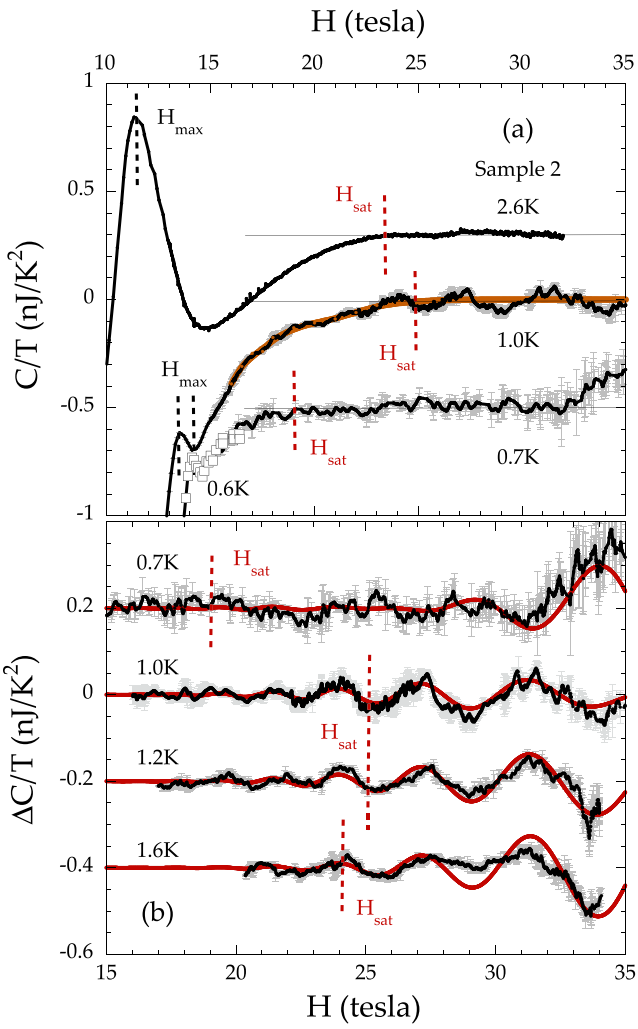

FIG. 6. (a) Field dependence of C/T in a FeSe single crystal (sample 2) for the indicated temperatures ($H\|c$); the different curves have been arbitrarily shifted for clarity. A (smeared) superconducting jump is visible for $H \sim H_{\rm max}$, and C/T still increases above the transition saturating for $H \sim H_{\rm sat}$. Quantum oscillations are clearly visible around 1 K. (b) highlights the presence of those quantum oscillations (for the indicated temperatures) after subtraction of a smooth background [solid brown line in (a)]. The red lines are fits to the data using the standard Lifshitz-Koshelev model (see text for details). Note that the oscillations are observed well below $H_{\rm sat}$ for $T \sim 1$ K, indicating that $H_{\rm sat}$ lies within the normal state.

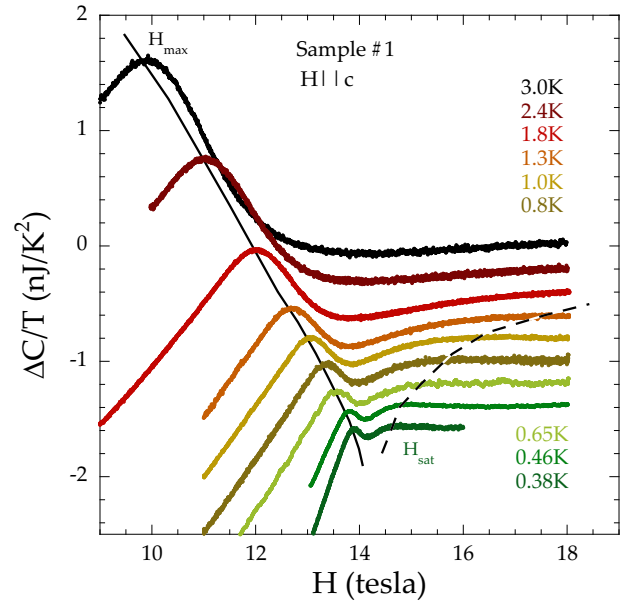

FIG. 7. Magnetic field dependence of the specific heat in FeSe single crystals (sample 1) at the indicated temperatures for $H||c$. The different curves have been arbitrarily shifted for clarity. As shown, a minimum develops above $H_{\rm max}$ (solid line), and C/T saturates for only $H > H_{\rm sat}$ (dashed line). The two lines seem to converge around ~14.2 T for $T \to 0$.

However, it is important to note that the jump observed for low θ values is very similar to the one observed for $\theta \to 90^\circ$ but is superimposed to a decrease of C/T below $H_{\rm sat}$ for $\theta \lesssim 50^\circ$ [thin red to yellow curves in Fig. 5(a)]. In Fig. 5(b), the red to yellow curves have been subtracted from the data to further emphasize the similarity of the transitions for both $\theta \to 0^\circ$ and $\theta \to 90^\circ$.

Consistently, $H_{\rm max}(\theta)$ can be very well described by an $H_{\rm max}(\theta) = H_{\rm max}^{||ab}/\sqrt{[\tilde{\gamma}\cos(\theta)]^2 + [\sin(\theta)]^2}$ law [see the solid line in Fig. 5(c)], as expected for the upper critical field in the anisotropic Ginzburg-Landau model [19]. However, $\tilde{\gamma} \sim 2$ is significantly smaller than the γ value observed for the melting line close to T_c ($\gamma \sim 4.5$; see Fig. 4), clearly indicating the presence of paramagnetic effects which reduce H_{c2} at low temperature [7] (especially for $H||ab$). The angular dependence of the upper critical field in the presence of those paramagnetic effects [30] is then expected to vary as

$$H_{\rm max}(\theta) = \frac{H_{\rm orb}^{||ab}}{\sqrt{[\gamma\cos(\theta)]^2 + [\sin(\theta)]^2 + 2.4(\alpha_M/2)^2}},$$

where α_M is the Maki parameter (for $H||ab$). This expression also perfectly reproduces the data with $\alpha_M \sim 3.1$ and an orbital critical field $H_{\rm orb}^{||ab}(T = 1.8\,{\rm K}) \sim 65$ T in very reasonable agreement with the value inferred above from the melting lines at $T = 0$ [$H_{\rm orb}^{||ab}(0) \sim 75$ T; see the discussion above]. One then consistently obtains $H_{c2}^{||c}(0) = H_{\rm orb}^{||c}(0) \times \gamma/\sqrt{\gamma^2 + 5.7} \sim 14.7$ T, further confirming that $H_{\rm max}$ lies close to the upper critical field at low temperature. Note that those values are slightly smaller than those previously inferred in [7] ($H_{\rm orb}^{||ab} \sim 90$ T and $\alpha_M \sim 4.4$) which also lead to a very reasonable fit to the data, assuming, however, that $\gamma \sim 5.8$.

C. Quantum oscillations

For $H||c$, the (smeared) superconducting jump at $H = H_{\rm max}$ and the increase of C/T up to $H = H_{\rm sat}$ are visible down to the lowest temperatures [see Figs. 6(a) and 7]. Moreover, quantum oscillations (QOs) are definitely observed above ~19 T for $T \sim 1$ K [see Fig. 6(a)]. To emphasize those QOs a smooth background [solid brown line in Fig. 6(a)] has been subtracted from the data displayed in Fig. 6(b). The oscillations can be well described by the Lifshitz-Kosevich formula [31] [solid red lines in Fig. 6(b)] taking an effective mass $m^* \sim 4m_e$ and a frequency $F \sim 200$ T. These (F, m^*)

values are in good agreement with those inferred from transport measurements [32,33] for the minimal cross section of the hole sheet. Similarly, an $F = 200$ T frequency has also been obtained in tunnel diode oscillator measurements [34] but with a smaller m^* value. Although of similar amplitude in transport data [32,33], the $F \sim 700$ T frequency oscillations associated with the maximal cross section of this sheet could not be resolved here because no warping term had to be introduced in order to fit the data (a fast Fourier transform analysis confirmed that no other frequency could be unambiguously extracted from the data). Note that the QOs in C/T are expected to change sign for $T[\mathrm{K}]/B[\mathrm{T}] \sim 0.11 \times m_e/m^*$ in the Lifshitz-Kosevich formalism, and the absence of clear QOs below 30 T at 0.7 K is then a direct consequence of this π-phase shift of the oscillations, which is expected to occur at $B \sim 25$–30 T for $T = 0.7$ K and $m^* \sim 4m_e$. Finally, note that those oscillations are observed above ∼19 T for $T \sim 1$ K, i.e., well below the saturation field $H_{\mathrm{sat}} \sim 24$ T, without introducing any extra damping factor, again clearly indicating that the normal state is reached below H_{sat}.

We did not observe the QOs associated with the electron sheet. In this case, a very small frequency ($F = 60$ T) was observed for its minimal cross section [32]. This orbit is expected to appear around ∼30 T (corresponding to $n = 2$ occupied Landau levels) and ∼20 T ($n = 3$), i.e., for H close to H_{sat}, and it might be tempting to associate the field dependence observed in C/T in this field range with those low-frequency oscillations. However, the Lifshitz-Kosevich formula would not be applicable for such small n values, and the Landau levels would show up as very distinct features instead of smooth oscillations (see, for instance, [18] for graphite close to the $n = 1$ quantum limit). Moreover, in the case of the hole sheet, the absence of QOs below 30 T at 0.7 K is a direct consequence of the large $m^* \sim 4m_e$ effective mass, and those features would still be clearly visible at low T for an electron sheet of lower effective mass ($m^* \sim 2m_e$). We did not observe the $F \sim 600$ T QOs associated with the maximal cross section of this electron sheet [32,33], probably due to its very large effective mass.

D. Saturation field and concluding remarks

We have shown that two distinct structures are visible in the field dependence of the specific heat at low temperature. First, a (smeared) superconducting jump is visible for $H \sim H_{\mathrm{max}}$ down to the lowest temperatures for both $H||c$ and $H||ab$. Surprisingly, for $H||c$, C/T still increases above the superconducting transition, finally saturating only above $H_{\mathrm{sat}} \gg H_{\mathrm{max}}$ (for $T \sim 1$–3 K). In striking contrast to H_{max}, for which the angular dependence can be well described by the standard $H_{c2}(\theta)$ law for anisotropic superconductors (in the presence of paramagnetic effects), H_{sat} only very weakly depends on the angle θ between the magnetic field and the c axis. H_{sat} then becomes smaller than H_{max} for $\theta \to 90°$, leading to a structure in $C/T(H)$ within the superconducting state, reminiscent of those observed in [8,11] for the latter field orientation [blue triangles and lozenges in Fig. 4(b)].

The origin of a second characteristic field H_{sat} (below which the specific heat of the normal state decreases) is a puzzling issue. For $H||c$, Kasahara *et al.* [10] recently reported the presence of a kink in $C/T(H)$ at low temperature around $H_{\mathrm{kink}} \sim 14.5$ T [see crossed squares in Fig. 4(b)]. Spectroscopic-imaging scanning tunneling microscopy indicated that the order parameter vanishes at the surface upon entering the high-field phase, and this kink has been interpreted as a transition within the superconducting state (see also [9]), consistent with the presence of a FFLO state. However, $H_{\mathrm{kink}} \sim H_{\mathrm{max}}$, and this kink is very likely reminiscent of the (smeared) jump observed here in $C/T(H)$ and hence of the superconducting transition itself. Note that H_{kink} lies slightly below the onset of the resistive transition [black squares in Fig. 4(b)], which can be attributed to the presence of small filamentary superconducting paths (due to sample inhomogeneities), bypassing the sample but invisible in bulk thermodynamical data. The vanishing of the order parameter for $H \sim H_{\mathrm{kink}} \sim H_{\mathrm{max}}$ then finds a straightforward explanation as $H_{\mathrm{max}} \sim H_{c2}^{\mathrm{MF}}$.

As pointed out above, no minimum is observed anymore in $C/T(H)$ for $\theta \to 90°$. However, a clear (small) change in slope remains visible around ∼24 T [see the stars in Figs. 3(b) and 5]. This kink can most likely be attributed to H_{sat}, which is only slightly angular dependent (in contrast to H_{max}), increasing from ∼22–23 T for $H||c$ at $T = 1.8$ K (hence being much larger than H_{max}) up to ∼23–24 T for $H||ab$, hence lying within the superconducting state close to the ab plane (scenario B in Fig. 1). The field dependence of the normal state specific heat then remains visible within the superconducting state due to the large amount of normal state in the vortex cores.

Note that this kink (i.e., the continuation of H_{sat} in the superconducting state) is in agreement with structures that were previously observed in irreversible torque and magnetocaloric measurements [8,11] for θ close to 90° [see blue triangles and lozenges in Fig. 4(b)]. Our specific heat data here confirm the presence of those anomalies through thermodynamic reversible measurements. Ok *et al.* also reported the presence of a second (low-T) torque anomaly around 15 T [11] which is not visible in our data. It was recently shown that this 15 T anomaly strongly depends on the sample quality and is observed only in samples with $T_c \sim 9$ K (see the Supplemental Material in [35]). The absence of any thermodynamic signature corresponding to this anomaly in sample 1 ($T_c = 8.1$ K) is hence consistent with this study, but still we did not observe any anomaly in sample 2, even though its $T_c = 9.0$ K. In [11], the authors attributed both anomalies to possible inherent spin-density-wave instabilities near the superconducting gap minima (or to a FFLO transition). Magnetic Lifshitz transitions have been discarded because they are set by the electronic structure and are thus expected to occur even in the normal state, which was not observed in their experiments. However, our thermodynamic data suggest that the H_{sat} line does actually exist both below and above the superconducting transition for $\theta \lesssim 80°$, making this option possible.

To conclude, the complete temperature dependence of H_{max} and H_{sat} is displayed in Fig. 7 [in sample 1 as an example; see also Fig. 6(a)]. As shown, H_{sat} decreases with T at low temperature, again indicating that it cannot be related to the superconducting transition. However, H_{sat} seemingly tends towards H_{max} for $T \to 0$ (solid and dashed lines in Fig. 7),

suggesting a relationship between the two anomalies for $T = 0$ which still has to be understood. Finally, note that H_{max} only weakly depends on T_c (decreasing by ∼4% from sample 2 to sample 1; see Fig. 3), whereas H_{sat} drops from ∼24–25 T at 1 K in sample 2 to ∼16–17 T in sample 1 (see Figs. 6 and 7). This would, at first glance, seem to suggest a significant change in the electronic structure leading to a decrease both in T_c and in H_{sat}. However, angle-resolved photoemission spectroscopy indicated that the decrease in T_c is not related to any significant change in the electronic structure, and it has been attributed to disorder [36], hence suggesting that H_{sat} could also be sensitive to disorder.

ACKNOWLEDGMENT

We acknowledge the support from LNCMI-CNRS, a member of the European Magnetic Field Laboratory (EMFL).

[1] G. R. Stewart, Rev. Mod. Phys. **83**, 1589 (2011).
[2] P. Dai, Rev. Mod. Phys. **87**, 855 (2015).
[3] Y. Bang and G. R. Stewart, J. Phys.: Condens. Matter **29**, 123003 (2017).
[4] S. Mukherjee, A. Kreisel, P. J. Hirschfeld, and B. M. Andersen, Phys. Rev. Lett. **115**, 026402 (2015).
[5] L. Fanfarillo, J. Mansart, P. Toulemonde, H. Cercellier, P. Le Fevre, F. Bertran, B. Valenzuela, and L. Benfatto, Phys. Rev. B **94**, 155138 (2016).
[6] A. Fedorov, A. Yaresko, T. K. Kim, Y. Kushnirenko, E. Haubold, T. Wolf, M. Hoesch, A. Gruneis, B. Buchner, and S. V. Borisenko, Sci. Rep. **6**, 36834 (2016).
[7] F. Hardy, L. Doussoulin, T. Klein, M. He, A. Demuer, R. Willa, K. Willa, A.-A. Haghighirad, T. Wolf, M. Merz, C. Meingast, and C. Marcenat, Phys. Rev. Res. **2**, 033319 (2020).
[8] S. Kasahara, Y. Sato, S. Licciardello, M. Culo, S. Arsenijevic, T. Ottenbros, T. Tominaga, J. Boker, I. Eremin, T. Shibauchi, J. Wosnitza, N. E. Hussey, and Y. Matsuda, Phys. Rev. Lett. **124**, 107001 (2020).
[9] S. Kasahara, T. Watashige, T. Hanaguri, Y. Kohsaka, T. Yamashita, Y. Shimoyama, Y. Mizukami, R. Endo, H. Ikeda, K. Aoyama, T. Terashima, S. Uji, T. Wolf, H. von Lohneysen, T. Shibauchi, and Y. Matsuda, Proc. Natl. Acad. Sci. USA **111**, 16309 (2014).
[10] S. Kasahara, H. Suzuki, T. Machida, Y. Sato, Y. Ukai, H. Murayama, S. Suetsugu, Y. Kasahara, T. Shibauchi, T. Hanaguri, and Y. Matsuda, Phys. Rev. Lett. **127**, 257001 (2021).
[11] J. M. Ok, C. I. Kwon, Y. Kohama, J. S. You, S. K. Park, J.-H. Kim, Y. J. Jo, E. S. Choi, K. Kindo, W. Kang, K.-S. Kim, E. G. Moon, A. Gurevich, and J. S. Kim, Phys. Rev. B **101**, 224509 (2020).
[12] A. Ptok, K. J. Kapcia, A. Cichy, A. M. Oles, and P. Piekarz, Sci. Rep. **7**, 41979 (2017).
[13] D. Chareev, E. Osadchii, T. Kuzmicheva, J.-Y. Lin, S. Kuzmichev, O. Volkova, and A. Vasiliev, CrystEngComm **15**, 1989 (2013).
[14] A. E. Böhmer, F. Hardy, F. Eilers, D. Ernst, P. Adelmann, P. Schweiss, T. Wolf, and C. Meingast, Phys. Rev. B **87**, 180505(R) (2013).
[15] S. Karlsson, P. Strobel, A. Sulpice, C. Marcenat, M. Legendre, F. Gay, S. Pairis, O. Leynaud and P. Toulemonde, Supercond. Sci. Technol. **28**, 105009 (2015).
[16] H. Cercellier, P. Rodière, P. Toulemonde, C. Marcenat, and T. Klein, Phys. Rev. B **100**, 104516 (2019).
[17] M. Roulin, A. Junod, and E. Walker, Science **273**, 1210 (1996).
[18] C. Marcenat, T. Klein, D. LeBoeuf, A. Jaoui, G. Seyfarth, J. Kačmarčík, Y. Kohama, H. Cercellier, H. Aubin, K. Behnia, and B. Fauqué, Phys. Rev. Lett. **126**, 106801 (2021).
[19] G. Blatter, M. Y. Feigel'man, Y. B. Geshkenbein, A. I. Larkin, and V. M. Vinokur, Rev. Mod. Phys. **66**, 1125 (1994).
[20] G. P. Mikitik and E. H. Brandt, Phys. Rev. B **68**, 054509 (2003).
[21] T. Klein, A. Conde-Gallardo, J. Marcus, C. Escribe-Filippini, P. Samuely, P. Szabo, and A. G. M. Jansen, Phys. Rev. B **58**, 12411 (1998).
[22] G. Blatter and B. I. Ivlev, Phys. Rev. B **50**, 10272 (1994).
[23] Y. Yeshurun and A. P. Malozemoff, Phys. Rev. Lett. **60**, 2202 (1988).
[24] C. C. Almasan, M. C. de Andrade, Y. Dalichaouch, J. J. Neumeier, C. L. Seaman, M. B. Maple, R. P. Guertin, M. V. Kuric, and J. C. Garland, Phys. Rev. Lett. **69**, 3812 (1992).
[25] The presence of significant static disorder can, however, contribute to the lattice displacement [19], and a rather large α value (∼1.5) has been reported in (K, Ba)BiO_3 despite its small $G_i \sim 3.10^{-4}$ [I. Joumard, J. Marcus, T. Klein, and R. Cubitt, Phys. Rev. Lett. **82**, 4930 (1999)].
[26] T. Watashige, Y. Tsutsumi, T. Hanaguri, Y. Kohsaka, S. Kasahara, A. Furusaki, M. Sigrist, C. Meingast, T. Wolf, H. v. Löhneysen, T. Shibauchi, and Y. Matsuda, Phys. Rev. X **5**, 031022 (2015).
[27] D. Nakashima and R. Ikeda, Phys. Rev. B **106**, 024508 (2022).
[28] D. S. Fisher, M. P. A. Fisher, and D. A. Huse, Phys. Rev. B **43**, 130 (1991).
[29] A. K. Nguyen and A. Sudbo, Phys. Rev. B **58**, 2802 (1998); **60**, 15307 (1999).
[30] K. Machida and M. Ichioka, Phys. Rev. B **77**, 184515 (2008).
[31] S. C. Riggs, O. Vafek, J. B. Kemper, J. B. Betts, A. Migliori, F. F. Balakirev, W. N. Hardy, R. Liang, D. A. Bonn, and G. S. Boebinger, Nat. Phys. **7**, 332 (2011).
[32] T. Terashima, N. Kikugawa, A. Kiswandhi, E.-S. Choi, J. S. Brooks, S. Kasahara, T. Watashige, H. Ikeda, T. Shibauchi, Y. Matsuda, T. Wolf, A. E. Bohmer, F. Hardy, C. Meingast, H. v. Lohneysen, M.-T. Suzuki, R. Arita, and S. Uji, Phys. Rev. B **90**, 144517 (2014).
[33] M. D. Watson, T. K. Kim, A. A. Haghighirad, N. R. Davies, A. McCollam, A. Narayanan, S. F. Blake, Y. L. Chen, S. Ghannadzadeh, A. J. Schofield, M. Hoesch, C. Meingast, T. Wolf, and A. I. Coldea, Phys. Rev. B **91**, 155106 (2015).
[34] A. Audouard, F. Duc, L. Drigo, P. Toulemonde, S. Karlsson, P. Strobel, and A. Sulpice, Europhys. Lett. **109**, 27003 (2015).
[35] N. Zhou, Y. Sun, C. Y. Xi, Z. S. Wang, J. L. Zhang, Y. Zhang, Y. F. Zhang, C. Q. Xu, Y. Q. Pan, J. J. Feng, Y. Meng, X. L. Yi, L. Pi, T. Tamegai, X. Xing, and Z. Shi, Phys. Rev. B **104**, L140504 (2021).
[36] Y. Sun, S. Kittaka, S. Nakamura, T. Sakakibara, P. Zhang, S. Shin, K. Irie, T. Nomoto, K. Machida, J. Chen, and T. Tamegai, Phys. Rev. B **98**, 064505 (2018).